Design of a Tiltrotor Semi-Span Wind Tunnel Model for Whirl Flutter Investigations

Stefan van 't Hoff[1] and Jelmer van Vilsteren[2]
Royal Netherlands Aerospace Centre (NLR), Amsterdam, Noord-Holland, Netherlands

Alessandro Cocco[3] and Pierangelo Masarati[4]
Politecnico di Milano, Milano, Lombardia, Italy

The Clean Sky 2 Advanced Testbed for TILtrotor Aeroelastics (ATTILA) project is aimed at the design, manufacturing and testing of a semi-span aeroelastic wind tunnel model of the Next Generation Civil TiltRotor (NGCTR). This paper provides a description of the ATTILA tiltrotor whirl flutter testbed design, as well as the design and test methodology and associated numerical modelling. In advance of the first wind tunnel test entry, the design activities rely on multi-level code-to-code validation as presented herein to improve confidence in the flutter predictions. The available numerical tools have been used to tailor the design to the desired flutter characteristics in the presence of the limitations associated with testing in Froude-scale conditions. Robustness of the predictions and design is investigated through parametric variations associated with modelling assumptions and design features. Finally, an outlook on the future dynamic characterization and wind tunnel test activities is provided.

I. Introduction

With the technological push from the European Clean Sky 2 Fast Rotorcraft project and the US Army Future Vertical Lift (FVL) program, both civil and military tiltrotor aircraft capabilities continue to expand while the technology remains under careful evaluation for a range of applications. Tiltrotor aircraft combine vertical take-off and landing capability with a speed, range and acceleration akin to that of modern turboprop airplanes, offering significant strategic advantage in a military environment, as well as promising efficient air mobility for the civil market [1]. The first flying tiltrotor aircraft prototype, the Transcendental Model 1-G completed about 100 flight hours from 1954 to 1955 without ever completing a full conversion [2]. Amongst other prototype aircraft, the Bell XV-3 in the 1950s [3] and the Bell XV-15 in the 1980s [2] enabled further technology maturation leading up to the successful development and continued military operation of the Bell-Boeing V-22 [4]. In recent years, Bell has been developing its V-280 Valor military tiltrotor which is the company's bid for the US Army Future Long-Range Assault Aircraft (FLRAA) program [5]. The Bell-Agusta and now Leonardo AW609 [6] is currently under development, aiming at the introduction of tiltrotor technology on the civil market [7,8].

Nevertheless, tiltrotor design remains a challenging engineering task, considering the various operating conditions and multipurpose missions that are expected to be accomplished by this type of aircraft. With the power trade-off between hover and high-speed cruise, the fundamental limitation on the tiltrotor maximum flight speed is not the available power, but a prevailing high-speed rotor-on-wing aeroelastic instability known as proprotor whirl flutter. The fundamental understanding and numerical modelling of the complex interplay between the aerodynamic forces and the elastic motion of the flexible wing-pylon, proprotor blades, control system, downstop mechanism and drive system remains one of the foremost challenges in tiltrotor aircraft design and development. Extensive experimental investigations are required, both for development purposes and certification compliance demonstration.

The NASA/Army/Bell 1/5-scale Wing and Rotor Aeroelastic Test System (WRATS), initially designed and tested as the JVX model from 1983 through mid-1988, has seen extensive aeroelastic testing in Froude and Mach-scale

[1] Senior R&D Engineer, Vertical Flight & Aeroacoustics Department.
[2] R&D Engineer, Engineering & Technical Services Department.
[3] Ph.D. Student, Department of Aerospace Science and Technology.
[4] Professor, Department of Aerospace Science and Technology.

conditions including parametric variations of key structural characteristics [9-10]. The TILTAERO and ADYN Mach-scaled tests [11] in the DNW Large Low-speed Facility (LLF) investigated the aerodynamic performance and aeroelastic stability of the ERICA tiltrotor concept [12]. Meanwhile, the US Army and NASA are pursuing continued generic tiltrotor aeroelastic research with the TiltRotor Aeroelastic Stability Testbed (TRAST) [13,17] which will accommodate both a gimballed and hingeless rotor. The Maryland Tiltrotor Rig (MTR) is another contemporary tiltrotor test rig that has been developed at the University of Maryland [18-20] and has recently been subjected to preliminary whirl-flutter stability tests [21,22].

In Europe, a parallel effort is underway in the Clean Sky 2 ATTILA project coordinated by NLR, which endeavors to design, build and test the Advanced Testbed for Tiltrotor Aeroelastics (ATTILA). The ATTILA testbed is a Froude-scale representation of the Next-Gen Civil Tilt Rotor (NGCTR) and consists of a cantilevered semi-span wing with powered rotor and instrumented pylon. The testbed is designed to enable testing in air in the DNW Large Low-speed Facility (LLF) in the 6 m × 6 m test section, as well as in heavy-gas at Mach-scaled conditions in the NASA Transonic Dynamics Tunnel (TDT) at some future date. Preliminary numerical modelling efforts and related aeroelastic stability predictions are presented in [23-25]. The current paper provides more details about the design and intended usage of the ATTILA testbed, and presents updated pre-test numerical aeroelastic stability predictions obtained using the multibody dynamics models developed within the project.

II. Wind Tunnel Testbed Design

A. Design Overview

The ATTILA wind tunnel testbed has been designed as a Froude-scale half-wing representation of the NGCTR under development in the Clean Sky 2 Fast Rotorcraft program [26]. The testbed design represents a trade-off between the modularity required in light of anticipated future NGCTR design iterations, the desire to minimize overall complexity and nonlinearities in the structural dynamics of the system, and the timeline and limited resources available for a program of this complexity. In the context of the ATTILA project, testing is scheduled to be performed across two entries in the Large Low-speed Facility (LLF) of the German-Dutch Wind Tunnels (DNW) in the Netherlands in 2023. Looking ahead, the design criteria also foresee testing in heavy-gas in the NASA Transonic Dynamics Tunnel (TDT) in Mach-scaled conditions. The testing in the LLF is primarily aimed at generating experimental data for the validation of the numerical tools used for the prediction of proprotor aeroelastic stability prior to high-speed flight testing of the NGCTR Technology Demonstrator in 2024 [27].

The ATTILA testbed shown in Fig. 1 features a stiff in-plane 1.25 m (4.1 ft) radius three-bladed constant-velocity gimballed rotor with flexured hub, mounted on a 1.8 m (5.9 ft) semi-span wing. The rotor is powered by a water-cooled 17.5 kW (23.5 hp) brushless DC electric motor situated in the tiltable part of the nacelle, obviating the need for a through-wing driveshaft and split 90-degrees gearbox. The wing root is directly cantilevered to the test section floor/wall and consists of an aeroelastically tailored rectangular carbon fiber beam, eight structurally isolated airfoil segments, and numerous adjustable non-structural masses (NSM). Considering the initial test purposes, the ailerons and large-chord moveable foreseen on the NGCTR are currently not included on the testbed.

Due to rotorhead mass and volume limitations and constraints imposed by the pitch control system it was not possible to incorporate a rotating shaft balance [28]. Instead, the wing-nacelle bracket features a decoupled six-component load balance that measures all aerodynamic loads except for those on the nacelle fairing. Rotor torque is measured by an instrumented flex-coupling installed in front of the gearbox. Redundant measurement of the in-plane hub forces is provided by strain instrumentation on the rotor mast. Beyond the load measurement capability, the torque flex-coupling and rotor load balance are primary design elements for tailoring the structural dynamics of the wing-pylon and drive train to match the full-scale reference. The layout of the rotor load balance is optimized for measurements in airplane mode; future operation in helicopter mode with tilted nacelle will require additional accommodations.

A remote-control downstop locking mechanism and parallel actuator spring restrain pylon tilt and enable in-situ pylon pitch and yaw stiffness tuning independently for the on-downstop and off-downstop configurations. To achieve pure wind milling operation, a retractable collar is mounted to the motor output shaft that enables decoupling the motor. Contrary to the experience on the WRATS and TRAST, powered operation is predicted to be significantly less stable than wind milling conditions for the ATTILA testbed. Pylon tilt is currently not included in the design, but is foreseen for future test configurations.

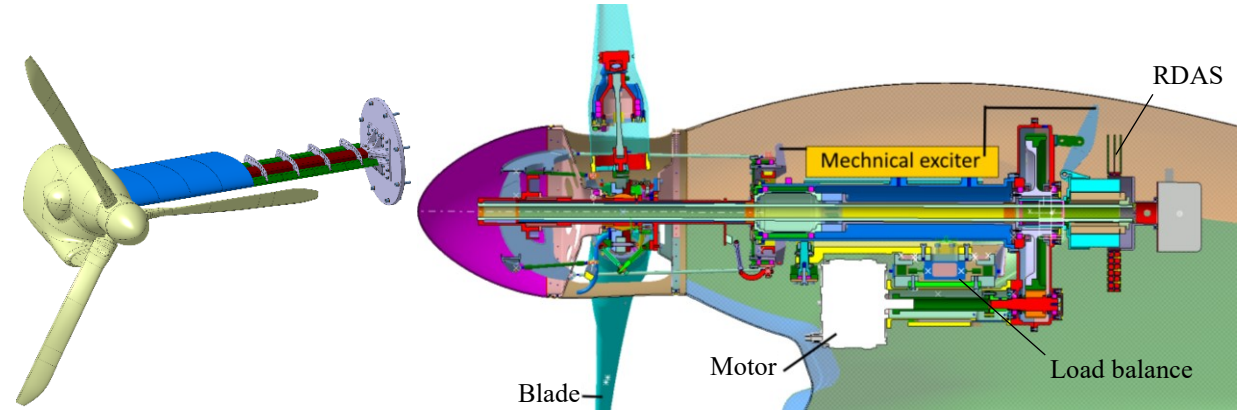

a) b)

Fig. 1 ATTILA testbed isometric view (a) and cut-through view of nacelle (b).

The proprotor blades are constructed from ultrathin-ply glass fiber fabric (0.045 mm) with a foam core and incorporate both conventional strain gauges and fiber optic sensors integrated in the D-spar for load measurement, safety of flight monitoring, and dynamic characterization. The same thin-ply glass laminate is also used for the yoke which provides the flexural flap and lag articulations and the physical interface for blade retention through a set of pitch-change bearings. Fig. 2 shows the ATTILA proprotor blade in its three consecutive manufacturing stages, prior to painting, with imbedded instrumentation visible at the D-spar.

The blade consists of a load-carrying D-spar structure at the front and a thin co-bonded airfoil section behind the D-spar. The D-spar geometry and composite layup has been tailored to replicate the target radial distribution of the blade elastic properties, aiming to match the target frequencies and mode shapes of at least the first five isolated blade modes. The inside of the D-spar is filled with a foam core to offer geometrical stability and prevent buckling of the (very) thin load-carrying laminates.

For a given (variable) chordwise dimension of the D-spar, the location of the neutral axis and shear center along the length of the blade is controlled through the number of reinforcement plies in the leading-edge of the D-spar and the vertical web. Furthermore, the design includes distributed NSM in the form of small chordwise-oriented tungsten bars to reproduce the desired blade mass distribution and chordwise and spanwise center of gravity. To ensure adequate curing pressure and enable intermediate visual inspection of the D-spar, a two-step manufacturing approach was adopted, in which the trailing-edge section is co-bonded in the second step.

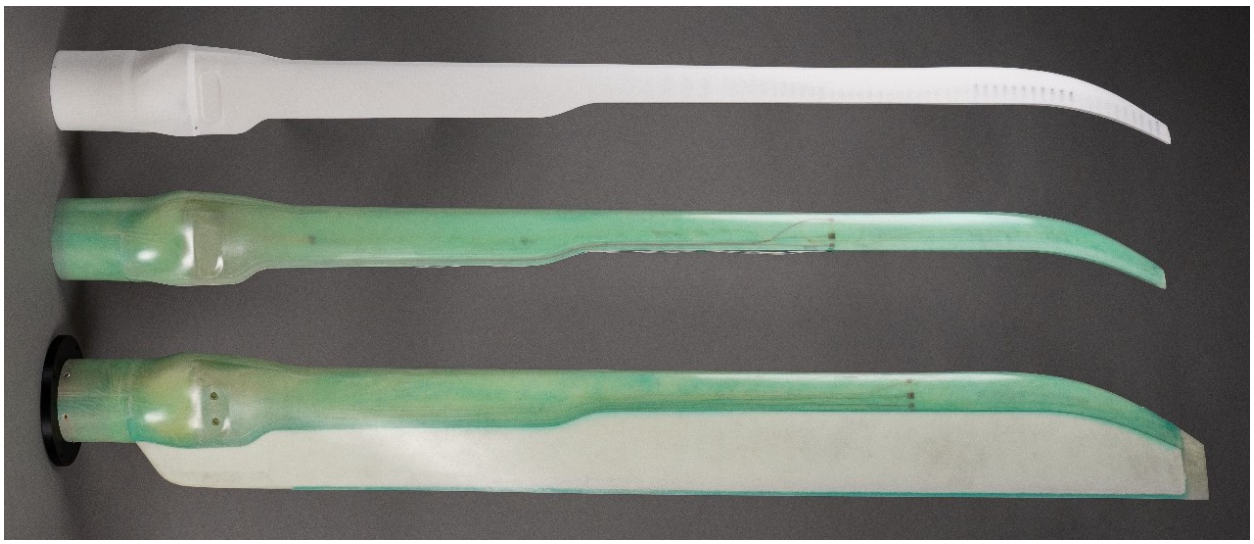

Fig. 2 ATTILA proprotor blade foam core, laminated D-spar, and complete blade including solid-laminate tip, strain instrumentation and yoke attachment.

The outboard bearing assembly shown in Fig. 3 isolates the yoke from flap and lag bending moments through a universal joint located at the radial station of the blade attachment pins and reacts the centrifugal loads via a set of three aerospace series spherical ball bearings. The inboard bearing assembly restrains flap and lag displacement, enabling free rotation and axial displacement at the blade root. Proprotor blade pitch control is achieved through a cyclic swashplate below the rotor and a rise-and-fall collective head assembly inside the spinner. The collective head is mounted on a rotating collective tube that extends through the drive shaft and gearbox and is translated by a lever attached to the housing of the annular digital slip ring. Translation of the collective head produces a collective blade pitch control input through a collective lever mechanism attached to the blade pitch links and the cyclic swashplate links. This design reflects that of the full-scale aircraft and was favored over a simpler conventional swashplate in order to achieve rotor couplings that are representative of the NGCTR across the full collective range. Design tuning of the stiffness of particularly the collective pitch control chain necessitated detailed finite-element analysis to achieve the desired frequency placement and derive the associated stiffness properties and modal mass.

In initial design iterations the Rotating Data Acquisition System (RDAS) was located in the rotorhead, incorporating robust contactless power and data transfer [29]. However, it was found that the forward placement of the associated mass led to a significant increase of the modal mass of the wing torsion mode and, consequently, affected the aeroelastic damping of said mode. Ultimately, it was decided to switch to a light-weight annular digital slip ring mounted at the bottom of the collective tube at the aft end of the nacelle. Similar weight and center of gravity considerations lead to the forward-oriented mounting of the electric motor as shown in Fig. 1, resulting in a nacelle center of gravity closer to the pylon tilt axis than would otherwise have been the case. In light of the proximity between the RDAS and the electric motor, the design of the RDAS electronics and associated cabling includes specific measures to reduce the emission of, and susceptibility to, electromagnetic interference such as the addition of a plastic coupling at the motor output shaft.

Independent trim-excitation units mounted on the tiltable pylon provide full-range trim pitch control and 0-25 Hz variable-amplitude sinusoidal flutter excitation inputs on all three control axes. The system was conceived as a fully electric self-contained, low-cost, low-weight design solution incorporating both functions in a single unit, shown in Fig. 3. The set-up comprises a walking beam arrangement that is attached to an exciter, a trim actuator, and an output shaft which is connected to either the collective or cyclic lever. The exciter consists of an eccentric pin driven by an electric motor that controls the excitation frequency. The eccentric pin is attached to a leaf spring disc on the other end; the orientation of the leaf spring disc, controlled by the amplitude actuator, determines the amplitude of the excitation. The system enables ramped amplitude excitation with rapid cut-off for free decay measurements and for use in case an unanticipated instability is encountered.

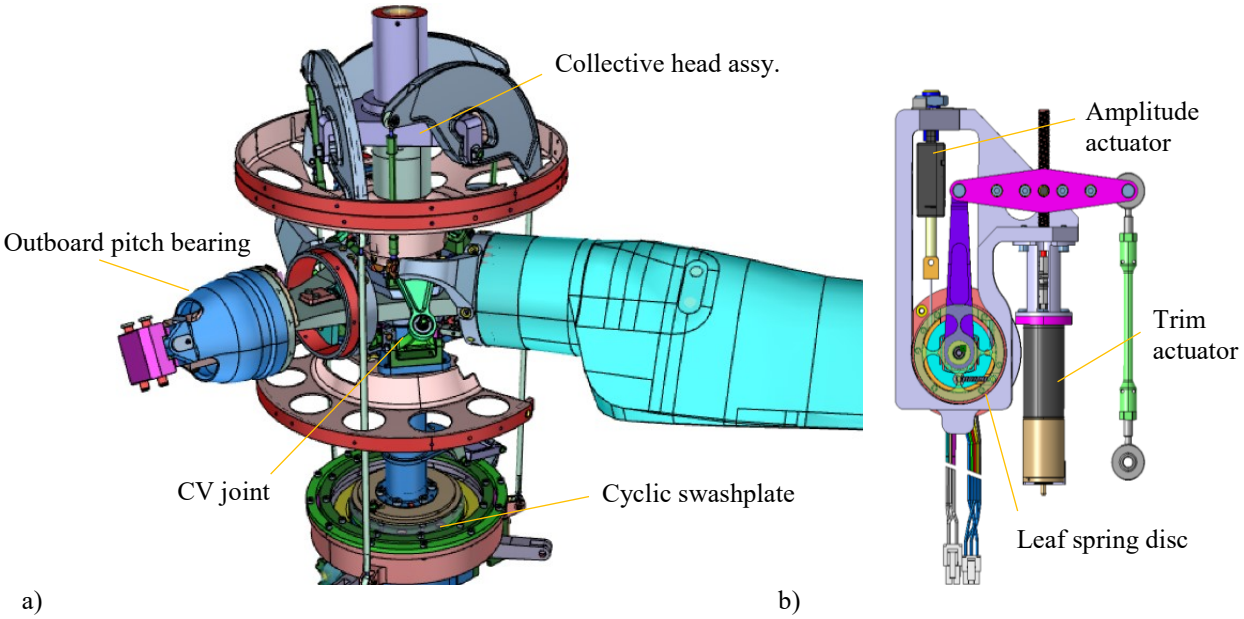

Fig. 3 ATTILA rotorhead design featuring constant-velocity (CV) joint, cyclic swashplate, rise-and-fall collective head assembly, and yoke-blade pitch bearing assembly (a), and trim-excitation unit (b).

DLR's Online Modal Analysis (OMA) system will be used for near real-time automatic and robust identification and extrapolation of the flutter mode frequencies and damping, Fig. 4 [30]. The primary sensors envisioned to be used for online modal analysis are the accelerometers mounted along the wing span and in the nacelle. A similar set-up has been used successfully for flutter tests of an elastic wing-body pylon nacelle wind tunnel model [31]. If the modal response due to forced excitation proves to be too small in comparison to the free stream turbulence and system vibrations, the wing root strain gauges may instead be used for assessment of the damping of the wing bending modes [17]. That being said, the primary flutter mode of interest for the ATTILA testbed is the wing torsion mode which has a considerable pylon pitch component that is dominated by rotation across the rotor load balance, suggesting that the load balance may provide a suitable alternative measurement for the damping assessment.

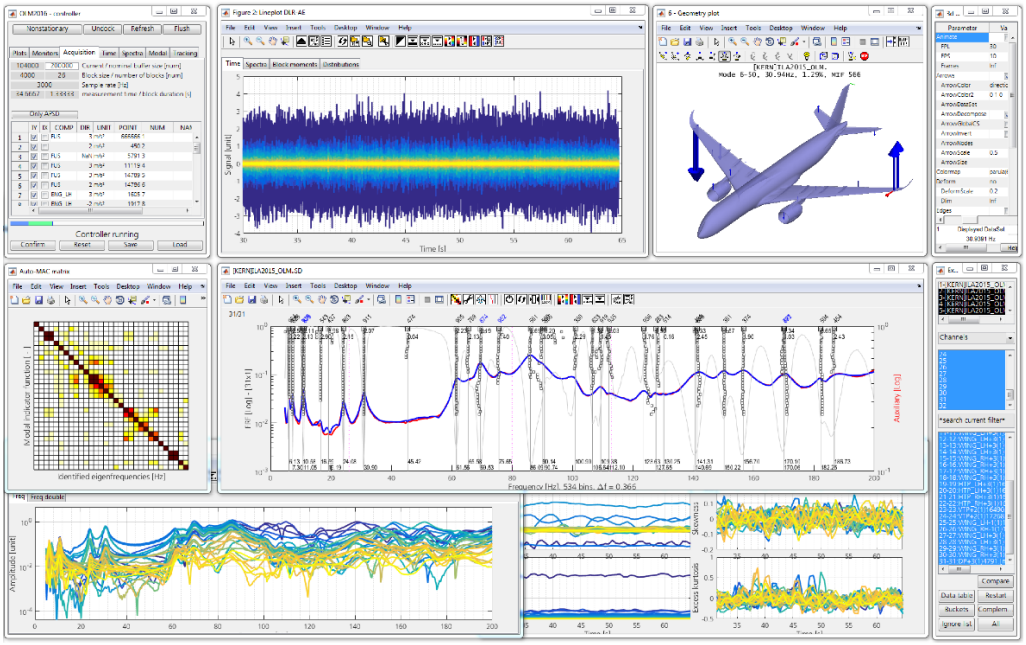

Fig. 4 Elements of GUI of the DLR Flight Vibration Testing modal analysis software (OLM).

B. Design and Test Methodology

The design activities in ATTILA revolve around a cascade of tools that translate the physical design to multibody dynamics models suitable for aeroelastic stability predictions. Through a number of design iterations and frequent mass distribution updates, the physical design in Catia and ABAQUS has first been converted to a detailed structural dynamics model in MSC NASTRAN, incorporating 3-D solid elements for those components that represent complex load paths, see Fig. 5. From this, a stick model was derived consisting of equivalent beam elements, springs, kinematic and distributing couplings, and lumped mass elements. The design and aeroelastic tailoring of the composite wing structures was accomplished entirely in ABAQUS and directly incorporated in the structural dynamics model. The stick model enabled rapid initial structural design evaluations, investigating different structural layouts and mass and stiffness tuning degrees of freedom. The primary focus of this effort was to match the full-scale NGCTR modal frequencies and the relevant components of the modal mass normalized hub mode shape of the fundamental wing-pylon modes involved in the proprotor whirl flutter instability.

The cross-sectional stiffness properties of the yoke and blade have been derived from the related ABAQUS models by applying, for each span station of interest, six unit loads to a clamped extruded section of the blade/yoke. The 6x6 sectional stiffness matrix is then deduced from the resulting deformations, correcting for displacements due to bending. Finally, the engineering stiffnesses of the cross-section (EA, EI_{yy}, EI_{zz}, GJ) and the locations of the neutral axis and shear center can be derived from this sectional stiffness matrix. The resulting beam descriptions are finally cross-validated with the original ABAQUS models to confirm the implementation as well as the suitability of the selected beam element discretization. That latter is not only important for obtaining the right dynamics, but also for accurate local structural or strain assessment along the length of the blade.

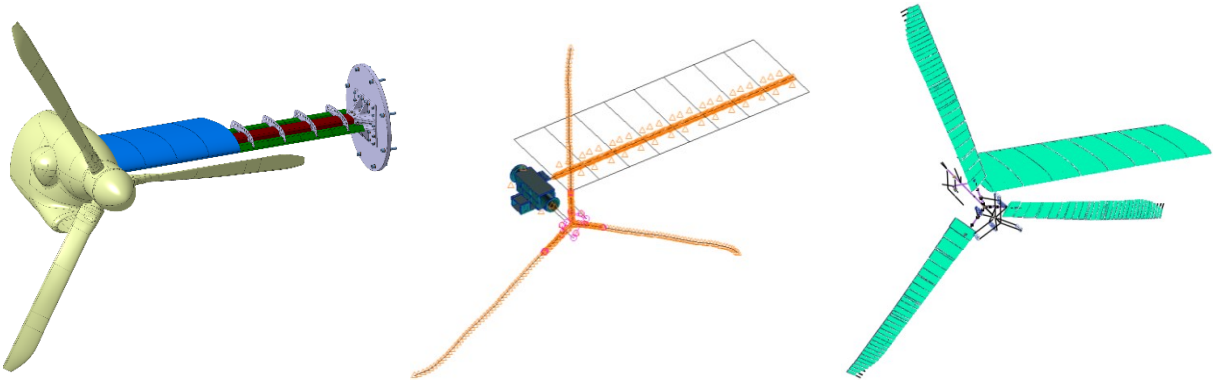

a) b) c)

Fig. 5 CAD model (a), 3-D NASTRAN model (b), FLIGHTLAB model (c).

To enable whirl flutter and rotor stability predictions as well as component-level structural load assessments, the NASTRAN stick model of the wing-pylon assembly was directly translated to equivalent finite-element beam models in FLIGHTLAB (https://flightlab.com/) and MBDyn ([24], https://mbdyn.org/). In these models, the rotor assembly lumped mass of the NASTRAN model was replaced by finite-element beam modelling of the yoke-blade assemblies as derived from the corresponding 3-D designs in ABAQUS. Along with appropriate aerodynamic modelling of the wing and rotor, as well as structural models for the pitch control and drive systems, the FLIGHTLAB and MBDyn models provide the means to predict the whirl flutter stability characteristics, investigate the effectiveness of the flutter excitation system, and derive design loads for structural substantiation for an otherwise stiffness-driven design. In a parallel effort, Leonardo Helicopters has developed an equivalent model in CAMRAD II to enable further cross-correlations.

As established in prior research [10,32], below the lift divergence Mach number, the effect of compressibility on the proprotor blade airfoil lift curve slope nominally results in a decrease of the whirl flutter stability limits for the same dynamic pressure. Similarly, the model-scale Reynolds number leads to a reduction in the lift curve slope and, consequently, to an increase in the predicted flutter boundary. The latter effect is particularly important for the Froude-scale tests in air in the DNW LLF. To account for these influences in the design stages, 2-D RANS CFD computations have been performed at full and model-scale conditions to derive blade and wing airfoil Reynolds number corrections to be applied to the available 2-D full-scale airfoil test data look-up tables. The corrections yielded an increase in the whirl flutter speed of nominally 10 knots.

The aforementioned Mach and Reynolds number effects meant that reproducing the full-scale flutter characteristics necessitated destabilizing modifications to the target model-scale structural dynamics of the ATTILA testbed. In practice, the mass penalties of the rotating data acquisition system and the pylon-mounted drive system made it impossible to achieve the desired flutter characteristics through modifications of the wing-pylon structure. Instead, acknowledging that the predicted damping of the wing torsion mode is strongly affected by the frequency placement of the regressive gimbal flap mode, tuning of the proprotor blade NSM distribution was selected as the most effective means by which the predicted flutter mode damping trends could be recovered. The flutter predictions presented in section V illustrate the prevailing sensitivities.

To support the structural substantiation of the critical components of the ATTILA testbed, transient response analyses were set up in FLIGHTLAB to replicate the anticipated experimental flutter excitation strategy. Single-axis proprotor collective and cyclic swashplate sinusoidal inputs at the frequencies of the wing-pylon modes were used to excite the modes of interest. The excitation magnitude was set to achieve desired predicted stabilized response amplitudes, quantified in terms of wing tip accelerations and wing root bending moments, based on prior flight and wind tunnel test experience. The resulting transient structural loads served as input for FEM-derived reduced order models that returned the predicted safety factors for the critical failure modes of the structure, enabling rapid trade-off assessments between the response amplitude desired for experimental damping measurements and the limits imposed by the structure.

Following the successful completion of the Critical Design Review mid-2022, the manufacturing, assembly and instrumentation are now underway. Build-up component and assembly-level static load and ground vibration testing has been started to enable dynamic characterization with specific emphasis on capturing the influence of key structural interfaces. The test data will feed back into the structural dynamics and multibody models to update the flutter predictions prior to the start of data gathering tests in the DNW LLF. Fig. 6 shows an example of a fixed-free ground

vibration test setup for the isolated yoke. Testing was also performed in free-free conditions, yielding a maximum difference in terms of frequency placement with respect to the FEM model of 2.5%. The predictive accuracy is considered more than satisfactory considering the difficulty of estimating the through-thickness stiffness of such a relatively thick solid-laminate part. This accuracy was achievable because of extensive material characterization coupon tests, as well as by virtue of the fact that the yoke was machined to its final dimensions following measurement of the fiber volume fraction after curing. Furthermore, the test activity confirmed minimal arm-to-arm differences in the stiffness properties, the desire for which was the leading motivation for the application of the ultrathin-ply glass fiber fabric.

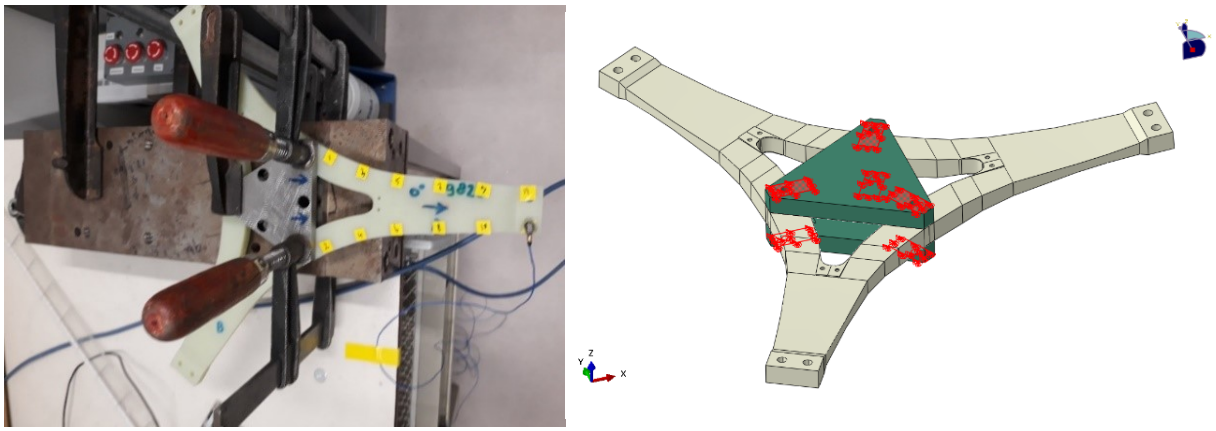

a) b)

Fig. 6 Composite yoke in fixed-free ground vibration test set-up (a) and associated CAD model (b).

III. Multibody Models

A. Wing-Pylon

The wing-pylon models in FLIGHTLAB and MBDyn are code-equivalents of the structural dynamics stick model in NASTRAN.

1. FLIGHTLAB

In FLIGHTLAB the wing and pylon are modelled using non-linear beam elements the formulation of which employs slender flexible beam assumptions, see Fig. 7. Concentrated mass components represent the airfoil segments, nacelle fairings and the other nonstructural wing and nacelle parts. The wing beam properties were derived from ABAQUS and include the clamping effects associated with the mounting of the airfoil segments. The lumped masses of the airfoil segments and mass tuning elements are assigned to the Aerodynamic Computation Points (ACPs) of the wing beam elements, thereby making the wing discretization independent of the large number of mass elements. In nominal configuration, the wing beam is rigidly cantilevered, which approximates the true interface. The root constraint combines a bolted connection, for structural strength, with adhesive bonding, to ensure predictable stiffness. An alternative model is available in which spring restraints at the wing root represent the equivalent stiffness of the wing root bracket attachment considering a pure bolted connection (i.e. after complete adhesive layer failure).

The first two beam elements outboard of the wing fairing represent the extension of the wing beam and the wing-nacelle bracket, respectively. The connection to the rotor load balance is modelled as a rigid 3-D offset. The load balance itself is represented by a series connection of three translational springs, followed by three rotational springs. To avoid a singular matrix during linearization, the mass of the balance is explicitly modelled and connected to the child side of the outermost spring element. The balance is connected to the controllable pylon tilt hinge via another rigid offset. The tilt hinge is connected on the child side to the downstop gimbal spring that represents the stiffness of the downstop mechanism, which itself is not modelled explicitly. The pitch and yaw stiffness of the gimbal spring that represents the downstop can be changed at run-time to switch between the on-downstop and off-downstop configurations. The downstop gimbal has two children that, respectively, rotate the local beam axis in aft and forward direction. The former then connects to a beam segment that represents the flexibility of the gearbox. The latter connects to the first beam element of the pylon leading towards the rotor node.

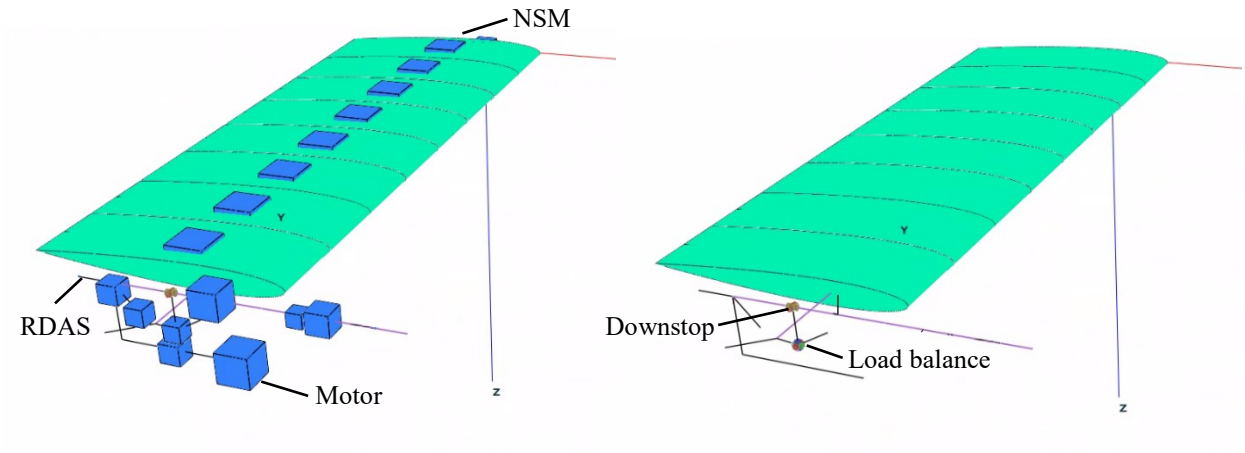

Fig. 7 FLIGHTLAB representation of ATTILA wing-pylon with (a) and without (b) mass components indicated.

The remainder of the pylon is modelled by a number of beam elements and lumped masses that represent the mass of, e.g., the cyclic swashplate, the collective swashplate mass, and the mass of the pylon itself. The aft beam element that represents the gearbox is connected via rigid offsets to the lumped masses that represent the electric motor and its output shaft. The mass of the RDAS and the remaining elements that translate with collective input are connected to the pylon through controlled sliders that adjust the position of the center of gravity of the associated elements in dependence of the collective input.

The wing airloads are captured using a lifting line model with a Peters-He finite-state wake. Rotor-wing aerodynamic interference effects are, for the moment, excluded. Each structural beam segment is connected to a spanwise aerodynamic segment that uses 2-D table look-up (angle of attack, and Mach/Reynolds number) to calculate the quasi-steady airloads. The wing aerodynamic segments use the full-scale airfoil aerodynamic look-up table corrected for Reynolds number effects (which are small for the wing). The default wing lift deficiency factor of 0.95 is applied, taking no specific account of the presence of the nacelle at the wing tip. The aerodynamic drag forces on the spinner and nacelle are neglected.

2. MBDyn

The wing model uses 3 finite volume three-node beam elements [33,34] for the stiffness part, for a total of 6 segments and 7 nodes. The inertial properties are modeled using a lumped inertia element for each node. The nacelle comprises a tilting and a non-tilting part, both modeled as rigid bodies, connected to one another and to the wing tip by deformable joints that represent the flexibility of the downstop and wing-pylon attachment. The aerodynamic loads are introduced through MBDyn's built-in aerodynamic beam elements, based on simple strip theory, each linked to the corresponding structural element.

B. Rotor Assembly

1. FLIGHTLAB

The rotor assembly consists of the yoke, three blades and the control chain. The yoke and blade are represented by means of the same nonlinear beam elements used for the wing. The blade elastic axis is staggered in the local chordwise direction to approximate the radial locus of shear centers. Nodes are placed at locations where large radial changes in physical properties occur. In addition, nodes have been added at critical strain locations for the on-line computation of the associated safety factors, based on strain relations derived from ABAQUS. The aerodynamics of the blade are modelled by means of table look-up with a correction for unsteady circulatory effects and the aforementioned Reynolds number effects. The rotor inflow modelling depends on the application, but in most cases an unsteady uniform inflow model was used, neglecting interactional effects.

The blade is connected to the yoke in two locations, at the inner bearing and at the outer bearing. To facilitate the dual load path introduced by the combination of the blade and the yoke, the root-end of the blade is modelled as a separate beam that is inverted, starting at the outer bearing, and connected at the physical root via the inner bearing. The inner bearing is represented using a zero-length 2-parent translational spring of practically infinite stiffness,

combined with a zero-length zero-stiffness 1-parent axial spring. The 2-parent translational spring has no inherent orientation and, therefore, restricts translational movement in all directions. The axial spring, connected in series with the translational springs, allows unrestrained movement in the local axial direction of the deformed yoke. To avoid numerical issues during linearization, the child node of the axial spring must have associated with it a non-zero mass; this is achieved by assigning the mass of the inner bearing to this node using a lumped mass component.

The outer bearing is modelled as a series of three one-dimensional torsional springs with zero spring stiffness, allowing rotation around all three axes while constraining translation. The pitch articulation is radially displaced from the collocated flap/lag hinges that represent the outer universal joint. The pitch bearing housing (see Fig. 3) is presumed to be infinitely stiff; the pitch articulation is accordingly modelled at the yoke-blade outboard attachment. In practice, the hinge order in the FLIGHTLAB model is inverted with respect to the design in that the pitch articulation occurs outboard of the flap/lag articulation. This adjustment has proven necessary for numerical robustness of the model. The effect on the rotor stability and load introduction into the yoke has been assessed, partly by relying on the ABAQUS model of the rotor assembly, and was found to be negligible.

To correctly capture the mass and inertia of the hub, pitch horn and pitch change bearings, associated concentrated mass elements have been defined and connected in their appropriate frames of reference. An additional mass is attached to the hub and is used to align the total rotor assembly mass and center of gravity with that of the NASTRAN structural dynamics model. Its mass includes, e.g., the mass of the spinner and the constant-velocity joint. The position is determined based on the difference between the target rotor assembly center of gravity and the nominal position derived by FLIGHTLAB at model initialization.

The pitch control chain is modelled as a conventional swashplate arrangement with appropriate collective and cyclic stiffness. A visual representation can be found in Fig. 8. The rotor hub is rigidly connected to the tip of the pylon when analyzing the half-wing model, and rigidly connected to the inertial system when analyzing the isolated rotor. The rotor speed bearing provides the rotor rotation to the gimbal and the swashplate. The swashplate is located above the hub, connected via a rigid offset. The non-rotating swashplate node is connected through a parallel arrangement of zero-stiffness dummy translation and gimbal rotation springs and three 2-parent translational springs. The stiffness of each of the 2-parent springs is equal to 1/3rd of the total collective stiffness. The cyclic stiffness is determined by the radial offset from the swashplate center as provided by the rigid translations.

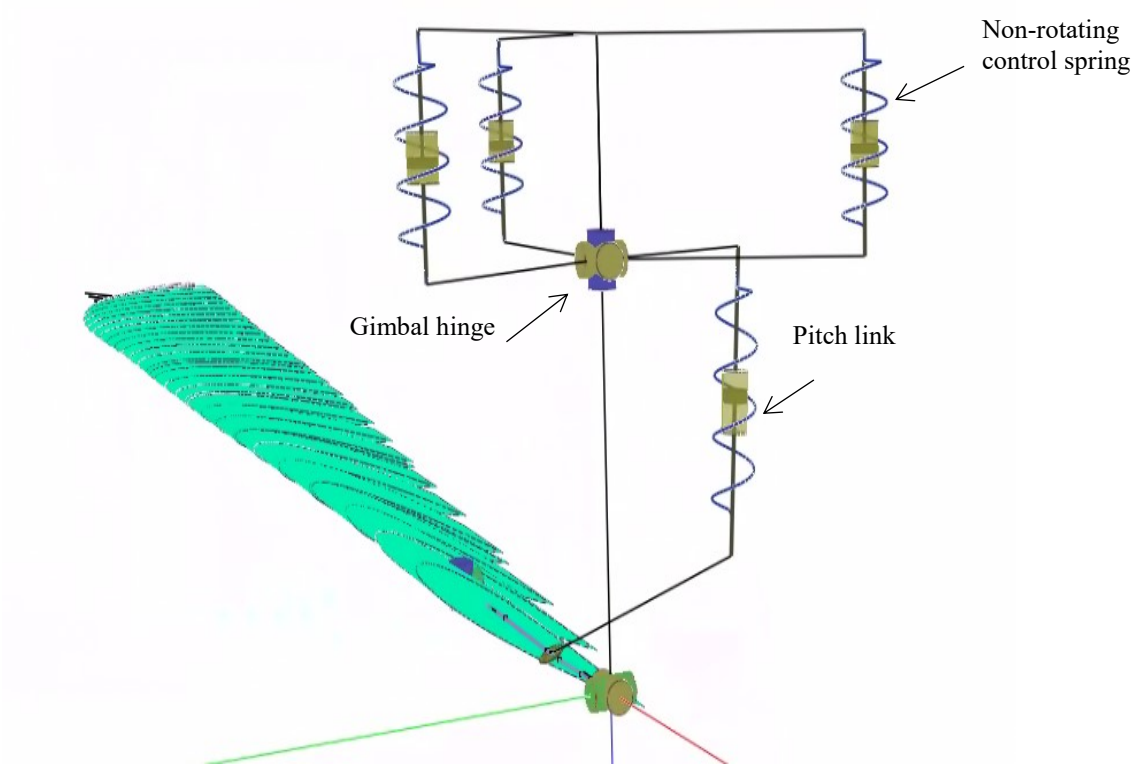

Fig. 8 Visual representation of custom FLIGHTLAB control chain model (one blade shown).

The collective mass is assigned to a dummy node which is attached to the parent side of the swashplate gimbal hinge. The cyclic mass is divided into a rotating and non-rotating part, both of which are assigned mass and inertia. The distribution of the inertia between the rotating and non-rotating part was observed to have a non-negligible influence on the frequency placement of the cyclic pitch mode.

An anti-mass (i.e. a negative mass) is connected on the parent side of the zero-stiffness dummy translation spring, thus translating with collective input without contributing to the collective control chain dynamics, with a mass equal to the sum of the swashplate cyclic and collective masses. This mass ensures that the collective and cyclic masses modelled in the rotorhead, independent of their translation due to control input, do not contribute to the wing-pylon dynamics (i.e., the net mass is equal to zero). Equivalent masses are attached along the length of the pylon at appropriate locations through controlled sliders that represent the movement of the collective head.

Azimuthal rotation of the rotating swashplate node is achieved by a controlled hinge, which is slaved to the rotational speed of the hub, prescribed by the rotor speed bearing component. Each pitch link is connected to the rotating swashplate and offset from the shaft through a constant azimuthal rotation and rigid translation. Cyclic control inputs are introduced at the root end of the pitch links through controlled sliders. A 2-parent linear spring-damper represents the pitch link stiffness and is connected to the pitch horn on the blade. The pitch link spring does not constrain rotation.

2. MBDyn

The flexible rotor is modeled in MBDyn using the same type of beam elements used for the wing. The blade and the yoke are both modeled as flexible elements. To account for the complex elastic properties of blade and yoke, the 6 by 6 stiffness matrix of the beam sections incorporate the offsets and relative orientations between the feathering axis and the neutral and elastic axes. The aerodynamics of the rotor are modeled using MBDyn's built-in aerodynamic beam element. Each aerodynamic panel incorporates aerodynamic chord and twist variation and changes of airfoil properties. Six airfoils are used along the blade, with a non-smooth transition.

The rotor aerodynamics are completed by a uniform inflow model, based on momentum theory, with empirical corrections for tip loss and other standard airflow and airloads correction features. Uniform inflow is deemed sufficient for supporting the design activities, taking into account the essentially axial flow operating condition at zero nacelle angle. This relatively simple model of the rotor aerodynamics is considered adequate in the tiltrotor aeromechanics literature for whirl-flutter predictions [35]. In an ongoing investigation, higher fidelity aerodynamics based on an original implementation of the Vortex-Particle Method (VPM) presented in [36] and tightly coupled to the MBDyn multibody simulation is being developed.

Each blade is connected to the yoke at the inner and outer bearing. In MBDyn, the two bearings are modeled with ideal rigid constraints: at the inner one, only flapwise and chordwise displacements are constrained, whereas the outer constrains all three components of displacement, as it is in charge of transferring the centrifugal loads from the blade to the yoke structure.

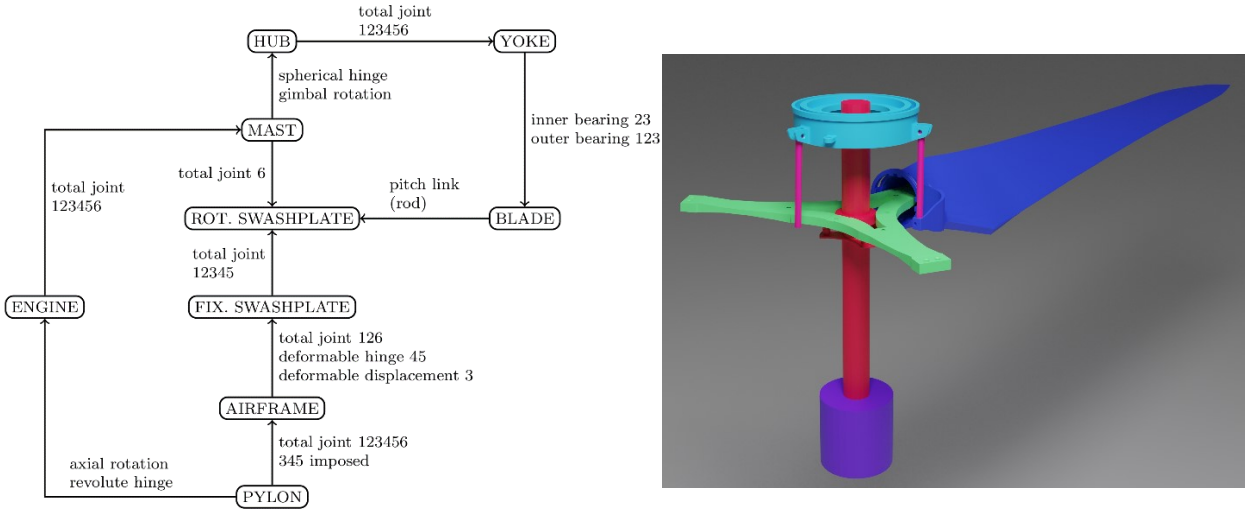

a) b)

Fig. 9 Layout of MBDyn control chain modelling (a) and illustration of MBDyn rotor model (b).

The control chain is modeled in detail and consists of seven nodes connected according to Fig. 9. The "Pylon" node connects the extremity of the pylon to the rotor; when the isolated rotor is analyzed, this node is clamped. The "Airframe" node receives the commanded collective and cyclic pitch controls and is rotated azimuthally by an angle that corresponds to the azimuthal location of the blade pitch link attachment with respect to the corresponding blade, thus decoupling the two cyclic inputs. The "Fixed Swashplate" node can only move vertically and tilt with respect to the airframe following collective and cyclic inputs, respectively.

To take into account the flexibility of the control chain, a collective spring, and two cyclic springs are positioned in between the airframe node and the fixed swashplate. The "Rotating Swashplate" node is connected to the fixed swashplate by a revolute hinge; its axial rotation is constrained in such a manner that it rotates along with the mast. The "Engine" node is connected to the mast by a torsional spring, to describe basic drive-train dynamics. The "Mast" node transmits the rotation to the hub and the rotating swashplate. It is connected to the pylon node by a revolute hinge. Finally, the "Hub" node is constrained to the mast node by a spherical hinge and a gimbal rotation constraint, creating an ideal constant-velocity (CV) joint.

IV. Code-to-Code Validation

Throughout the design activities code-to-code validation has been performed across the various models used to support the design. This includes comparisons between FLIGHTLAB and the 3-D FEM models in ABAQUS and NASTRAN in terms of the dynamic characteristics and local steady-state strain predictions of the yoke-blade assembly, and the non-rotating stiffness matrix and dynamic properties of the control chain. FLIGHTLAB, MBDyn and CAMRAD II were cross-validated in terms of wing-pylon and rotor – drive train dynamics, rotor elastic couplings, structural load predictions, trim blade deformations, and stability characteristics. Laboratory testing is currently underway to provide experimental confirmation of the predictions and/or provide information for required model updates.

Fig. 10 presents a comparison of the mass-normalized rotor hub mode shapes between the NASTRAN and FLIGHTLAB wing-pylon models. The NASTRAN model was used to tailor the structural wing-pylon design to the target frequencies and hub mode shapes. The rotor load balance stiffness was subsequently fine-tuned in the FLIGHTLAB model to obtain the desired whirl flutter characteristics, resulting in slight changes to the mode shapes and frequencies. In the NASTRAN model the rotor assembly is represented by a lumped mass rigidly connected to the pylon at the hub center. The FLIGHTLAB model incorporates the full gimballed rotor system in the form of finite element beams and distributed mass elements representing the pitch bearing and hub elements. The modal characteristics of the system are dependent on collective position owing to the considerable mass associated with the RDAS mounted at the bottom of the collective tube. Fig. 10 corresponds to the dynamics at maximum collective position.

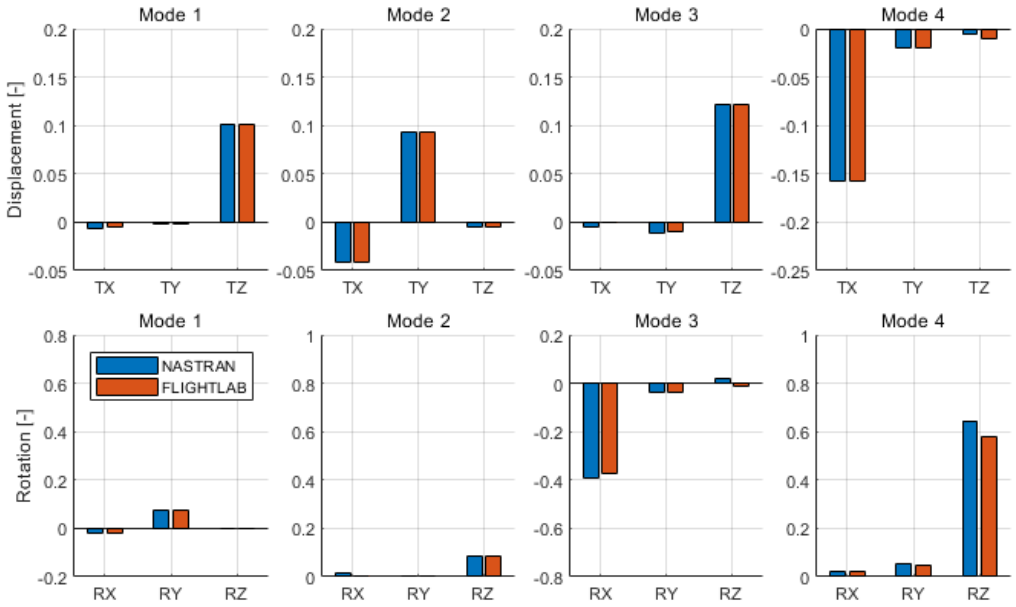

Fig. 10 Maximum-collective rotor hub mode shape normalized to unit modal mass as obtained from NASTRAN and FLIGHTLAB.

An example of the code-to-code correlation in the rotor mode frequencies is presented in Fig. 11, where the CAMRAD II results correspond to the dynamics of the reference model that was the design target and the FLIGHTLAB and MBDyn results reflect the ATTILA blade design. The figure demonstrates the level to which the ATTILA design replicates the desired isolated rotor dynamics and furthermore shows that excellent agreement is obtained between the codes, despite the complexity of the blade structure and hub retentions. The slight differences in the frequency placement of the cyclic pitch mode is accompanied by small discrepancies in the aerodynamic damping. Dynamic characterization tests are necessary to determine the associated structural damping, which is expected to be considerable for this particular mode in which the pitch control mechanism plays a dominant role. Additional comparisons in terms of mode shapes and associated rotor couplings lend further credibility to the predictions.

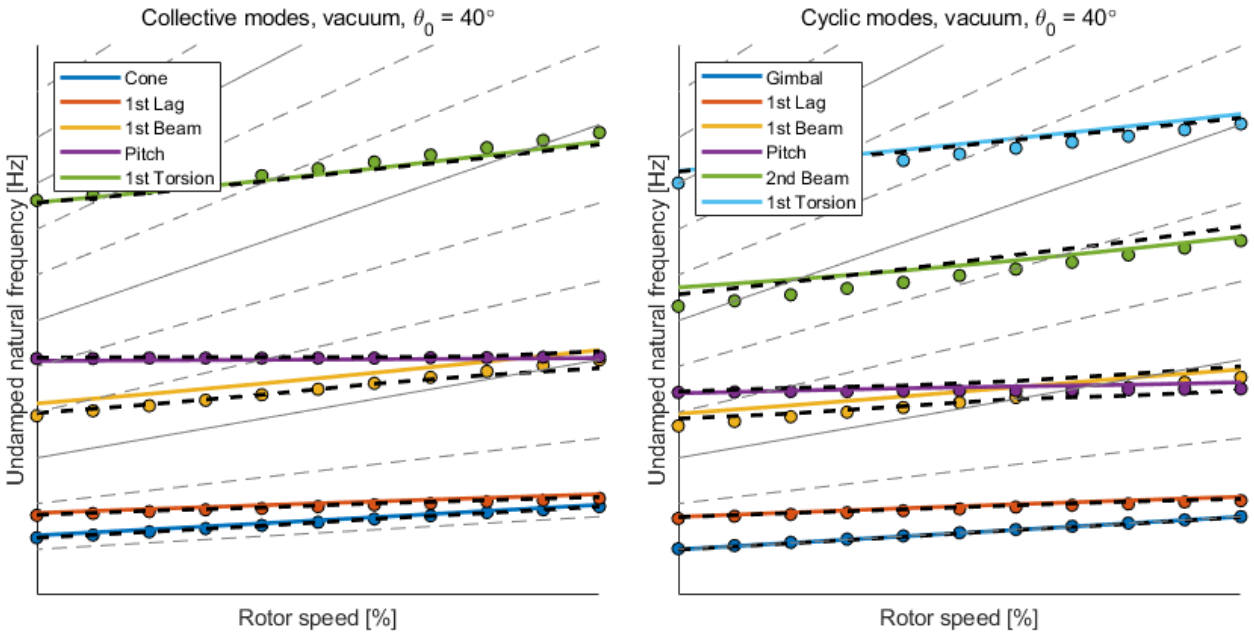

a) b)

Fig. 11 Comparison of predicted isolated rotor vacuum rotor mode frequencies at 40 degrees collective (CAMRAD II reference: colored markers, FLIGHTLAB: colored solid lines, MBDyn: black dashed lines).

V. Whirl Flutter Predictions

Throughout the project several methods for determining the whirl flutter characteristics of the ATTILA testbed have been investigated, particularly in MBDyn [25]. In FLIGHTLAB the default methodology relies on direct linearization by numerical perturbation of the state equations, providing information on both wing-pylon and rotor modes. In this case, a constant-torque linearization is achieved by excluding the solution component for engine and governor dynamics from the linearization. The solution thus obtained was verified by replicating in FLIGHTLAB the experimental excitation anticipated for the wind tunnel test activities and deriving the frequencies and damping of the fundamental flutter modes from the free decay response.

Beyond the assessment of the dynamic characteristics of the components and sub-assemblies that make up the ATTILA testbed, the primary drivers for the design have been the damping trends of the fundamental whirl flutter modes in comparison to the reference design. Having said that, the limitations of testing in Froude-scale conditions in air have necessitated compromises in the correlation with the full-scale design. To achieve the best possible trade-off, extensive effort was put into identifying the design variations that yielded maximum impact on the flutter characteristics with minimum effect on rotor dynamics and design complexity.

Fig. 12 and Fig. 13 demonstrate, respectively, the effectiveness of modifications in the blade NSM distribution and the kinematic δ_3 angle as determined by the pitch horn geometry. Both design modifications influence the damping of the wing-pylon modes through their effect on the frequency placement of the regressive lag and gimbal flap modes. In fact, the increase in gimbal flap mode frequency targeted here is of the same order of magnitude as that associated with the compressibility effects that are missing when testing in Froude-scale conditions.

The reduction in rotor NSM acts additionally to move the center of gravity of the nacelle further aft, closer to the full-scale target location. The net result is a significant destabilization of the wing torsion mode and a comparatively small influence on the damping of the chordwise mode, thus ensuring that the torsion mode remains the critical mode determining the flutter instability speed (in accordance with the full-scale design). In contrast, changes in blade pitch-flap coupling, or δ_3 angle, though effective in destabilizing the flutter characteristics, do not effectively separate the instability speed of the two wing-pylon modes. Moreover, the rotor dynamics are more sensitive to changes in δ_3 angle, thereby moving the wind tunnel model design further away from the full-scale target characteristics.

Other design modifications that have been investigated include changes to the nominal test rotor speed and pylon length. Both parameters are effective to some extent in destabilizing the wing torsion mode, but only in combination with a commensurate flattening of the damping trends. The latter is undesirable from a test-to-code validation perspective. Notably, the control chain collective stiffness was found to have a comparatively large effect on the chordwise bending mode damping, but the design offers flexibility to modify this stiffness in-situ through the replacement of a single link in the control chain.

In addition to the purpose of tailoring the whirl flutter characteristics, flutter analyses were devoted to investigating the sensitivity of the predicted characteristics to deviations in the properties of some of the key as-manufactured components, as well as to a potential failure of the adhesive bond layer at the wing root bracket. The latter was determined to result in a consequent decrease in the frequency placement of the beamwise and chordwise bending modes without significant detrimental impact on the associated damping trends.

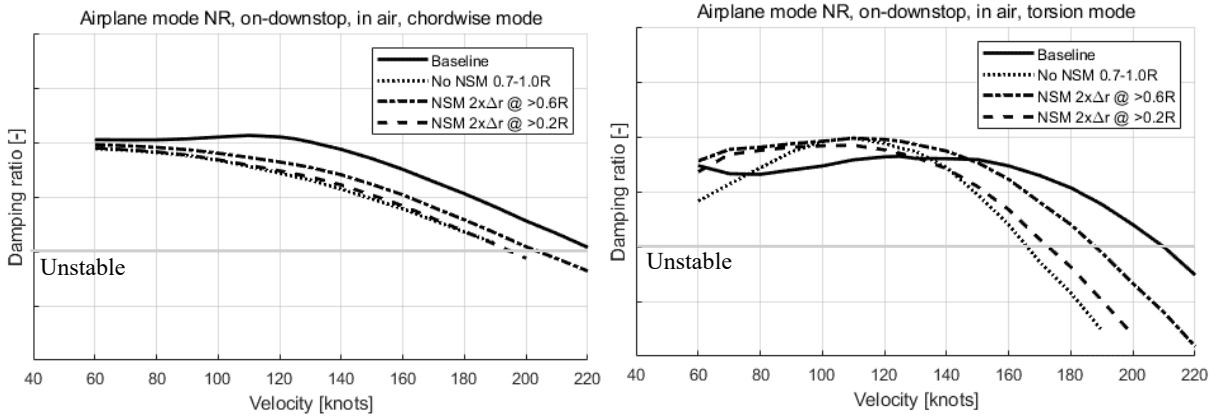

a) b)

Fig. 12 Influence of blade NSM distribution on FLIGHTLAB-predicted damping trends of wing torsion and chordwise bending modes.

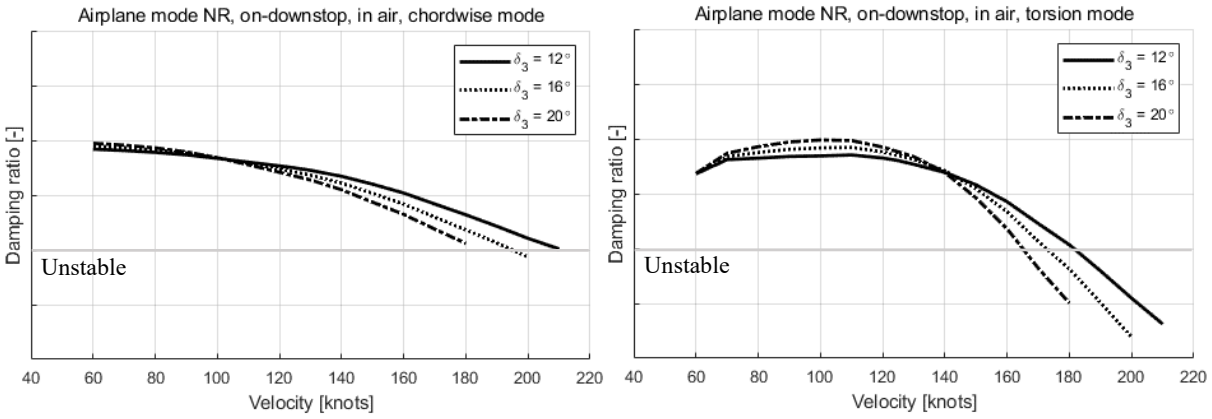

a) b)

Fig. 13 Influence of kinematic δ_3 angle on FLIGHTLAB-predicted damping trends of wing torsion and chordwise bending modes.

Fig. 14 shows the influence of changes in the rotor load balance stiffness on the damping trends of the wing torsion and pylon yaw modes. The analysis considers only reductions in stiffness because an inadvertent increase in balance stiffness can be recovered by adjustments of the downstop spring elements, both in on-downstop and off-downstop configurations. Reviewing Fig. 14, it is apparent that comparatively large manufacturing discrepancies would need to be encountered before appreciable effects on the instability speed are observed. Commensurately, such changes, if not corrected elsewhere, lead to appreciable reductions of the associated wing-pylon mode frequencies below the full-scale reference. In fact, the effect of the balance stiffness is sensitive to the nominal frequency placement with respect to the fundamental rotor modes and thus to the aforementioned modifications to the rotor system dynamics.

Finally, analyses were performed to verify the robustness of the tiltrotor whirl flutter stability predictions to variations in modelling assumptions. Fig. 15 shows that, amongst the model variants investigated, the wing tip loss effect correction is the only parameter of influence and that the only mode affected is the wing torsion. These observations are in line with the earlier assertion that relatively straightforward aerodynamic modelling is generally sufficient for the purpose of whirl flutter predictions. Accordingly, unsteady airfoil aerodynamic shed wake effects do not contribute significantly to the damping of the flutter modes for the conditions analyzed and modelling assumptions applied. Time-domain simulated flutter excitation analyses confirm these observations for the current level of modelling. The investigations using VPM modelling for the rotor and wing wake are ongoing and will be reported on in a future publication.

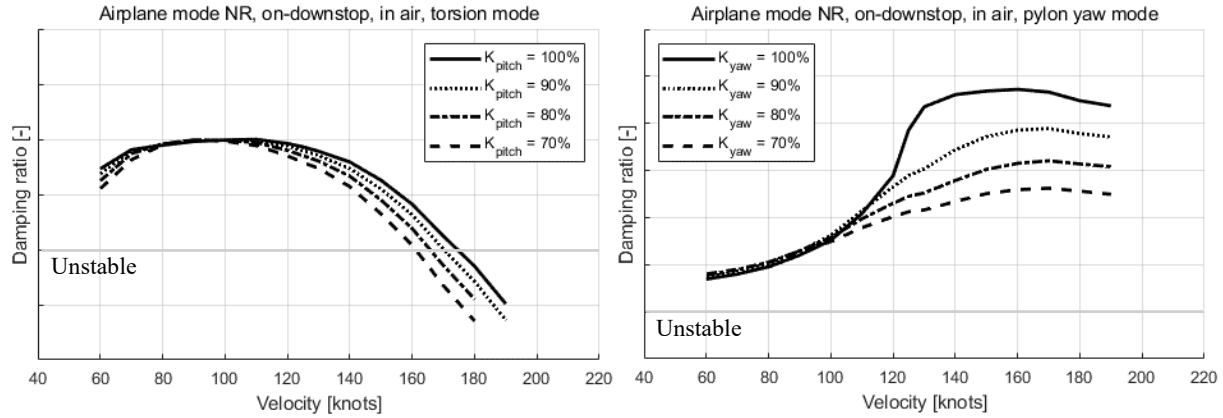

a) b)

Fig. 14 Influence of rotor load balance pitch/yaw stiffness, expressed as percentage of nominal design value, on FLIGHTLAB-predicted damping trends of wing torsion and pylon yaw modes.

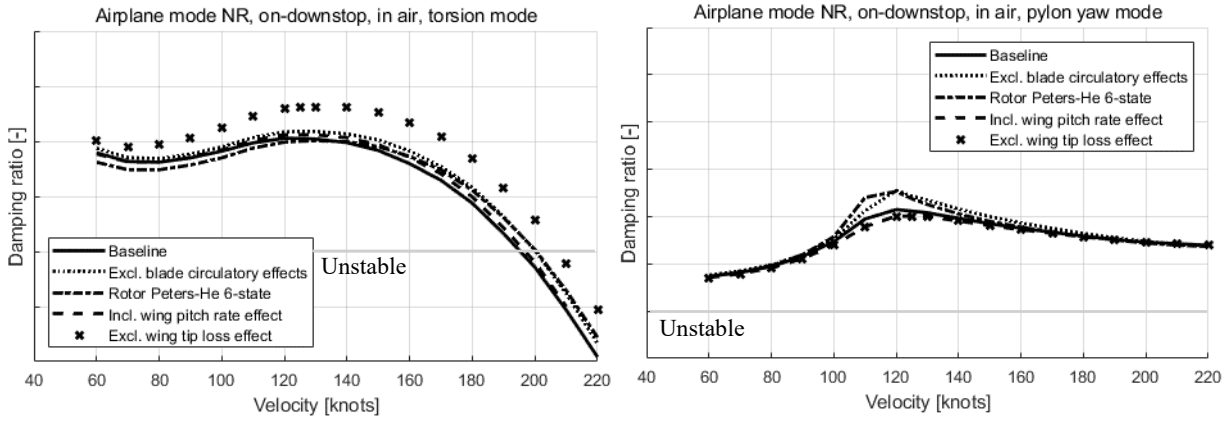

a) b)

Fig. 15 Influence of aerodynamic modelling assumptions on FLIGHTLAB-predicted damping trends of wing torsion and pylon yaw modes.

VI. Current Status and Near-Term Plans

At the time of writing, the manufacture of the ATTILA testbed is well underway. Initial component-level ground vibration tests indicate high correlation with the numerical models used to support the design. Further bench testing of the flutter excitation and electric drive system is planned prior to final assembly in Q1 2023. Thorough dynamic characterization testing is planned to underpin the numerical predictions, with an emphasis on characterizing the structural interfaces in the assembly and identifying potential nonlinearities that could affect the whirl flutter dynamics observed in the tunnel. Two separate test entries in the DNW LLF in the Netherlands are planned for the remainder of 2023, the first of which is primarily meant to shakedown the system. The second entry will be dedicated to data gathering.

Acknowledgments

This research received funding from the Clean Sky 2 – H2020 Framework Program, under grant agreement N. 863418 (the ATTILA project). The authors also acknowledge the valuable technical contributions provided by the Rotor Dynamics Department at Leonardo Helicopter Division, as well as the other partners in the ATTILA Consortium; DLR, DNW and PhotonFirst.

References

[1] Stevens, J., Rademaker, E., Scullion, C., Vouros, S., Nalianda, D., Pachidis, V., Van Oosten, N., Misté, G., Benini, E. and Venturelli, G., "Design Evaluation and Performance Assessment of Rotorcraft Technology by 2050," *45th European Rotorcraft Forum*, Warsaw, Poland, 2019.
doi: 10.3030/776900

[2] Maisel, M. D., Giulianetti, D. J., and Dugan, D. C., *The History of The XV-15 Tilt Rotor Research Aircraft - From Concept to Flight*, NASA SP-2000-4517, Monographs in Aerospace History #17, 2000.

[3] Deckert, W. H., and Ferry, R. G., "Limited Flight Evaluation of the XV-3 Aircraft," Report AFFTC-TR-60-4, Air Force Flight Test Center, 1960.

[4] Rosenstein, H., and Clark, R., "Aerodynamic Development of the V-22 Tilt Rotor," *12th European Rotorcraft Forum*, Garmisch-Partenkirchen, Germany, 1986.

[5] Ehinger, R., Gehler, C., and Allen, S., "Bell V-280 Valor: A JMR-TD Program Update," *Proceedings of the 73rd Annual Forum of the American Helicopter Society*, Fort Worth, TX, USA, 2017.

[6] Parham, T., Jr., and Corso, L. M., "Aeroelastic and Aeroservoelastic Stability of the BA 609," *25th European Rotorcraft Forum*, Rome, Italy, 1999, pp. G3–1–10.

[7] Fraser, W., King, D., Schaeffer, J. M., and Wells, D., "Development of Powered-Lift Airworthiness Standards as Applied to the AW609 Tiltrotor Certification Basis," *Proceedings of the 74th Annual Forum of the American Helicopter Society*, Phoenix, AZ, USA, 2018.

[8] ACARE— Report of the Group of Personalities, "European Aeronautics: a Vision for 2020," , January 2001.

[9] Settle, T.B. and Kidd, D.L., "Evolution and Test History of the V-22 0.2-Scale Aeroelastic Model", American Helicopter Society National Specialists' Meeting on Rotorcraft Dynamics, Arlington, Texas, 1989.

[10] Piatak, D. J., Kvaternik, R. G, Nixon, M. W., Langston, C. W., Singleton, J. D., Bennett, R. L. and Brown, R. K., "A Wind-Tunnel Parametric Investigation of Tiltrotor Whirl-Flutter Stability Boundaries," *Proceedings of the American Helicopter Society 57th Annual Form*, Washington DC, 2001, pp.184-196.
doi: 10.4050/JAHS.47.134

[11] Krüger, W. R., "Multibody analysis of whirl flutter stability on a tiltrotor wind tunnel model," *Proc. IMechE, Part K: J. of Multi-body Dynamics*, Vol. 230, No. 2, 2016, pp. 121–133.
doi:10.1177/1464419315582128.

[12] Nannoni, F., Giancamilli, G., and Cicalè, M., "ERICA: the European Advanced Tiltrotor," *27th European Rotorcraft Forum*, Moscow, Russia, 2001, pp. 55.1–15.

[13] Kreshock, A.R., Kang, H., Yeo, H., and Acree, C.W., "Development of a New Aeroelastic Tiltrotor Wind Tunnel Testbed", *Annual AIAA SciTech Forum*, San Diego, California, 2019.

[14] Yeo, H., and Kreshock, A. R., "Whirl Flutter Investigation of Hingeless Proprotors," *Journal of Aircraft*, Vol. 57, No. 4, 2020.
doi:10.2514/1.C035609.

[15] Kreshock, A.R., Thornburgh, R.P., Kang, H., Yeo, H., She, J. and Baggett, J., "Pretest Flutter Predictions of the Upcoming Aeroelastic Tiltrotor Wind Tunnel Test", *Vertical Flight Society's 76th Annual Forum*, Virtual, 2020.

[16] Yeo, H., Kang, H., and Kreshock, A. R., "Modeling and Analysis of Proprotor Whirl Flutter," *Vertical Flight Society's 77th Annual Forum & Technology Display*, Palm Beach, Florida, USA, 2021.

[17] Kreshock, A.R., Thornburgh, R.P. and Wilbur, M.L., "Overview of the TiltRotor Aeroelastic Stability Testbed", *Vertical AIAA SciTech Forum, San Diego, California*, 2022.

[18] Datta, A., Tsai, F., and Sutherland-Foggio, J., "Design of a New Tilt Rotor Test Facility at the University of Maryland," *AIAA SciTech 2019 Forum*, San Diego, CA, USA, 2019.

[19] Tsai, F., Sutherland-Foggio, J., Datta, A., , and Privett, D., "The Maryland Tiltrotor Rig (MTR): The Baseline Gimballed Hub," *Vertical Flight Society 75th Annual Forum*, Philadelphia, Pennsylvania, USA, 2019.
[20] Sutherland, J. R., and Datta, A., "Fabrication, Testing, and 3-D Comprehensive Analysis of Swept Tip Tiltrotor Blades," *Vertical Flight Society 77th Annual Forum*, Virtual, 2021.
[21] Sutherland, J. R., Tsai, F., and Datta, A., "Whirl Flutter Test of the Maryland Tiltrotor Rig: Swept-Tip Blades," *AIAA SciTech 2022 Forum, Dynamics Specialists Conference*, San Diego, CA, USA, 2022.
[22] Gul, S., and Datta, A., "Whirl Flutter Test of the Maryland Tiltrotor Rig: Prediction and Validation," *AIAA SciTech 2022 Forum, Dynamics Specialists Conference*, San Diego, CA, USA, 2022.
[23] Guerroni, F., Cocco, A., Zanoni, A., and Masarati, P., "Uncertainty Quantification of Tiltrotor Whirl Flutter Aeroelastic Stability from Multibody Analysis," *46th European Rotorcraft Forum*, Moskow, Russia, 2020.
[24] Masarati, P., Morandini, M., Mantegazza, P., "An Efficient Formulation for General-Purpose Multibody/Multiphysics Analysis", *Journal of Computational and Nonlinear Dynamics,* 9(4), 041001, 2014. doi:10.1115/1.4025628
[25] A. Cocco, S. Mazzetti, P. Masarati, S. van 't Hoff, B. Timmerman, "Numerical Whirl-Flutter Analysis of a Tiltrotor Semi-span Wind Tunnel Model", *CEAS Aeronautical Journal*, 13, pp. 923–938, 2022. doi:10.1007/s13272-022-00605-2.
[26] M. Hirshberg, "Clean Sky 2 Update, Part 2: The Leonardo Next Generation Civil Tiltrotor", *Vertiflite*, Vol.63, No. 6, 2017
[27] A.D. Marano, M. Belardo, J. Beretta,, F. Starace, S. Orlando, C. Punzi, R. Frajese, N. Paletta, and L. Di Palma, "Aeroelastic Tailoring of the Next Generation Civil Tiltrotor Technological Demonstrator Composite Wing", *Aerospace,* 9(7), 335, 2022. doi:10.3390/aerospace9070335.
[28] B.R. Nahuis and T. Sinnige, "Design, Manufacture and Commissioning of a New NLR Six-Component Rotating Shaft Balance for Delft University of Technology", *10th International Symposium on Strain Gauge Balances*, China Aerodynamics Research and Development Center, Mianyang, China, 2016.
[29] S.M. Bardet, R. Zwemmer, P.R. Faasse, J.I. de Goede, *A Contactless Telemetry System for a Contra-Rotating Open Rotor Test Campaign*, NLR-TP-2015-172, Amsterdam, Netherlands, 2015.
[30] G. Jelicic, J. Schwochow, Y. Govers, Yves, J. Sinske, R. Buchbach, J. Springer, "Online Monitoring of Aircraft Modal Parameters during Flight Test based on permanent Output-only Modal Analysis", *58th AIAA/ASCE/AHS/ASC Structures, Structural Dynamics, and Materials Conference*, Texas, USA, 2017. doi: 10.2514/6.2017-1825
[31] H.S. Timmermans, J.H. van Tongeren, E.G.M. Geurts, R.F.A. Marques, M.S. Correa, and S. Waitz, "Design and Validation of a Numerical High Aspect Ratio Aeroelastic Wind Tunnel Model (HMAE1)", *International Forum on Aeroelasticity and Structural Dynamics IFASD 2019*, Georgia, USA, 2019. doi: 10.3390/aerospace7110166
[32] Johnson, W., Lau, B.H. and Bowles, J.V., "Calculated Performance, Stability, and Maneuverability of High-Speed Tilting-Prop-Rotor Aircraft", NASA TM-88349, 1986.
[33] Ghiringhelli, G.L., Masarati, P., Mantegazza, P., "A Multi-Body Implementation of Finite Volume C^0 Beams", *AIAA Journal* 38(1), pp. 131–138, 2000. doi:10.2514/2.933
[34] Bauchau, O.A., Betsch, P., Cardona, A., Gerstmayr, J., Jonker, B., Masarati, P., Sonneville, V., "Validation of Flexible Multibody Dynamics Beam Formulations Using Benchmark Problems", *Multibody System Dynamics*, 37(1), pp. 29–48, 2016. doi:10.1007/s11044-016-9514-y
[35] W. Johnson, "Analytical Modeling Requirements for Tilting Proprotor Aircraft Dynamics", NASA TN D-8016, 1975.
[36] Savino, A., Cocco, A., Zanotti, A., Tugnoli, M., Masarati, P., Muscarello, V., "Coupling Mid-Fidelity Aerodynamics and Multibody Dynamics for the Aeroelastic Analysis of Rotary-Wing Aircraft Configurations", *Energies*, 14(21), 6979, 2021. doi:10.3390/en14216979